Journal of King Saud University – Science 33 (2021) 101443

Contents lists available at ScienceDirect

Journal of King Saud University – Science

journal homepage: www.sciencedirect.com

Original article

Effect of rare earth rubidium chloride on the optical, mechanical and antifungal behaviours of L-lysine monohydrochloride crystal for photonics and medical application

B. Aneeba [a,*], S.V. Ashvin Santhia [b], S. Vinu [c,*], Alaa Baazeem [d], R. Sheela Christy [b]

[a] Research Scholar, Register number: 18123112132045, Department of Physics and Research Centre, Nesamony Memorial Christian College, Marthandam, Affiliated to Manonmaniam Sundaranar University, Abisekapatti, Tirunelveli, 627012, TamilNadu, India
[b] Department of Physics and Research Centre, Nesamony Memorial Christian College, Marthandam, 629165, TamilNadu, India
[c] Department of Physics, Govt. Arts and Science College, Nagercoil, TamilNadu 629004, India
[d] Department of Biology, College of Science, Taif University, P.O. Box 11099, Taif 21944, Saudi Arabia

ARTICLE INFO

Article history:
Received 23 February 2021
Revised 4 April 2021
Accepted 8 April 2021
Available online 18 April 2021

Keywords:
Slow evaporation
Monoclinic
Optical material
Mechanical property

ABSTRACT

L-Lysine monohydrochloride and rubidium chloride doped L-Lysine monohydrochloride crystals with high optical, mechanical and antifungal were grown by slow evaporation techniques. The Single crystal XRD ascertained the monoclinic structure and the crystals were grown with lesser grain boundaries. Functional groups and existence of Rb was confirmed by FTIR and EDX. Grown crystals exhibit good transmittance than pure in UV–Visible region and the band gap of pure and doped crystals are 5.30 eV and 5.94 eV. Mechanical property of doped crystal was significantly improved due to RbCl doping and it lead the crystal for device fabrication. Nonlinear optical property of the grown crystals were surpassing than KDP and confirmed by Kurtz Perry technique. The Rb added crystal pronounced excessive inhibitory action towards pathogenic fungus like *Candida albicans*, *Candida parapsilosis* and *Aspergillus Flaves* than pure L-LMHCL crystal.
© 2021 The Author(s). Published by Elsevier B.V. on behalf of King Saud University. This is an open access article under the CC BY license (http://creativecommons.org/licenses/by/4.0/).

1. Introduction

In science and modern technology, optical crystals are significant in view of their technical importance mostly in the sector of photonics such as frequency conversion, modulators, laser technology, optical communication, computing, colour displays and high-speed information processing (Boopathi et al., 2016, Elamathi et al., 2020). Non-Centro symmetric materials play a major role in electro-optical applications, which is also a desirable ambience for second harmonic generation (Kandhan et al., 2020, Yusof et al., 2020, Ravi et al., 2021). Excluding glycine, all the amino acids hold a non-centro symmetric space group (Kandasamy et al., 2008). L-Lysine monohydrochloride (L-LMHCL) is one of the amino acid based non-Centro symmetric semi organic material. The stability and durability of materials are enriched by Rubidium chloride (Rb). Therefore, rubidium is applied in the field of optical fibre telecommunication networks, photomultiplier tubes, biomedical research and solar panels are used as an insulator in the ceramic sector owing to its large dielectric constant (Ertan, 2017 & Fan et al., 2020). Incorporation of Rb cation enhanced the electrical conductivity and diode characteristics of methylammonium lead iodide PSCs (Park et al., 2017). Piezoelectric and ferroelectric properties were increased by rubidium when doped with potassium- sodium-niobate crystals (Kimura et al., 2010). It has an impact on the membrane of bacteria, which intimates the antibacterial activity of rubidium (Ouyang et al., 2020). Rb does not cause any undesirable side effect in the human body and animals (Fieve et al., 1971). Manic-depressive illness of human being is also reduced by the intaking desirable amount of Rb (Paschalis et al., 1978, Malek-Ahmadi and Williams 1984). Lucia et al have been delineated the enrichment behaviours of rubidium chloride doped L-alanine hydrogen chloride monohydrate crystal likes dielectric and mechanical properties (Lucia Rose et al., 2011). So in this paper, an attempt is made to dope the alkali halide RbCl into L- LMHCL to improve the optical, mechanical and antifungal prop-

* Corresponding authors.
E-mail addresses: aneebaanu@gmail.com (B. Aneeba), vinusnist@gmail.com (S. Vinu).
Peer review under responsibility of King Saud University.

Production and hosting by Elsevier

https://doi.org/10.1016/j.jksus.2021.101443
1018-3647/© 2021 The Author(s). Published by Elsevier B.V. on behalf of King Saud University.
This is an open access article under the CC BY license (http://creativecommons.org/licenses/by/4.0/).

erties and the characterization studies were carried out using different techniques.

2. Materials and method

2.1. Materials used

Using L-Lysine mono hydrochloride and rubidium chloride, which was purchased from Sigma Aldrich Chemicals, Rb: L-LMHCL and L-LMHCL crystals were grown. A solvent used in this process was deionised water.

2.2. Growth procedure

Rb: L-LMHCL crystal was grown in the molecular ratio 0.02:0.98 by adapting slow evaporation techniques. Using deionised water, the estimated amount of rubidium chloride and L-lysine mono hydrochloride were stirred persistently to achieve a homogeneous and saturated solution. It was kept at an ambient temperature condition for optimization of growth by slow evaporating. Growth procedure of pure crystal L-LMHCL also same as Rb: L-LMHCl. In the repetitive crystallization process, the purity of the crystals was improved. Optically transparent, colourless crystals of pure and Rb: L-LMHCL crystals were garnered after 30 days which are shown in Fig. 1a and b.

2.3. Characterization techniques

In order to explore the structure of the crystal ENRAF NONIUS CAD4 X-ray diffractometer was used. The diffraction peaks of finely powdered pure and Rb: L-LMHCL crystals was obtained at different 2θ angles using XPert Pro- P Analytic powder diffractometer. Thermo Nicolet Avatar 370 spectrometer was used in the 400–4000 cm^{-1} wavenumber range to scrutinize the functional groups present in grown crystals. The composition present in Rb: L-LMHCL was picked out using SIGMA HV – Carl Zeiss with Bruker Quantax 200 – Z10 EDS Detector). The optical performance and mechanical behaviours were confirmed by making use of Perkin Elmer (Lambda 35) and HMV-2T micro hardness tester. The NLO property of crystals were studied using Q-switched high energy Nd: YAG laser. Disc diffusion method was used to test the antimicrobial activities against fungus.

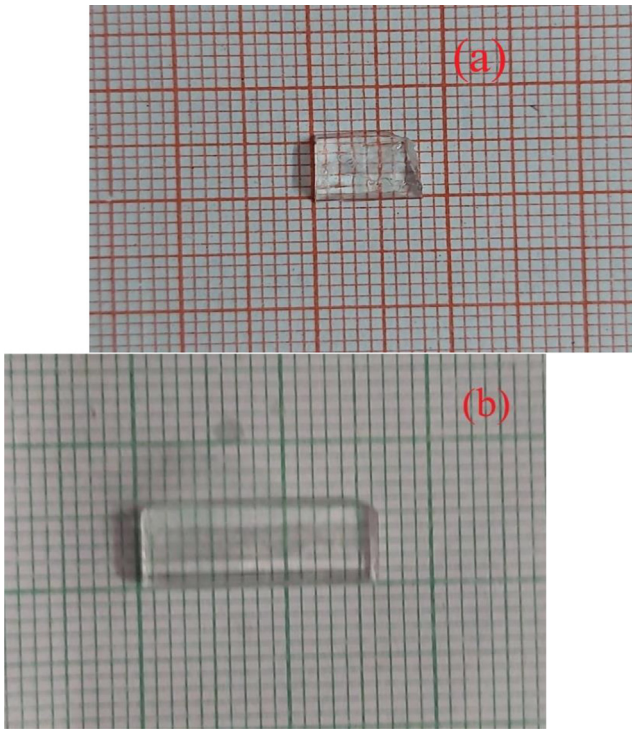

Fig. 1. Photograph of a) L-LMHCL and b) Rb: L-LMHCL crystals.

3. Results and discussion

3.1. XRD analysis

Fig. 2a shows the characteristic peak of XRD corresponding to the crystalline nature of pure and Rb: L- LMHCL, and 2θ angles 24.00, 24.66, 24.94 corresponding to planes (−121), (200), (210), respectively. No extra peaks in the Rb: L-LMHCL crystal compared to pure reveals the absence of secondary phases. The structure and the space groups of Rb: L-LMHCL are found out, with the influence of single crystal XRD. The lattice cell parameters such as a = 5.94 Å, b = 13.36 Å, c = 7.55 Å, α = γ = 90, β = 97.85 and V = 595 $Å^3$ ascribed monoclinic structure and $P2_1$ space group also analogue with the structure of pure L-LMHCL (Aneeba et al., 2020). Right shift of the prominent characteristic peak, the minute variation in lattice constants and FWHM (Fig. 2b) from pure are depicted that this is due to the effect of alkali metal halide (RbCl) using as dopant. As well as the increase in lattice parameter value and rise in intensity of doped crystal is due to the effect of Rb^+ ions. The high intensity diffraction peaks of Rb: L-LMHCL substantially discloses the quality of crystal and the smaller grain boundaries (Anis et al., 2018).

3.2. Vibrational analysis of Rb: L-LMHCL crystal

The finest way to elucidate the functional group of grown crystal is FTIR analysis. It was interpreted in the wave number range 400–4000 cm^{-1}. Fig. 3 shows the FTIR spectra of pure L-LMHCL and Rb: L-LMHCL crystal. The absorption band occurring at 3418 cm^{-1} was attributed to NH_3^+ asymmetric stretching vibration. The peak at 1406 cm^{-1} is owing to COO^- symmetric stretching. The band at 1612 cm^{-1} and 1506 cm^{-1} reveals the weak asymmetric and strong symmetric NH_3^+ bending vibrations. CH_2 twisting and COO^- wagging are ascribed in the range1347 cm^{-1} and 552 cm^{-1}. C–C stretching and O–H-O out of plane bending imputed

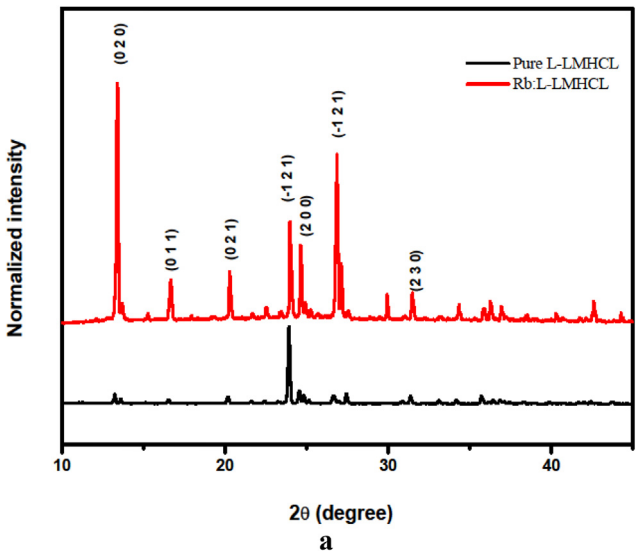

Fig. 2a. Powder XRD pattern of pure and Rb: L-LMHCL crystals.

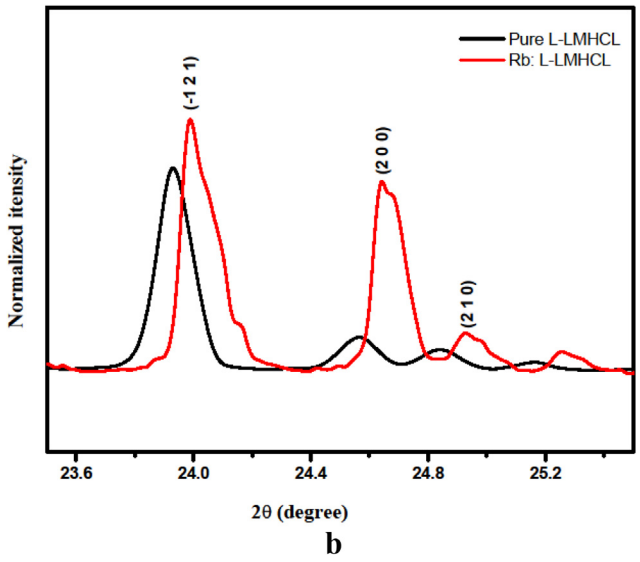

Fig. 2b. Variation of peak intensity and shifting of pure and Rb: L-LMHCL crystals.

at 995 cm^{-1} and 861 cm^{-1}. The peak at 1143 cm^{-1} noticed the NH_2 and NH_3 rocking. The vibrational bands of pure and doped crystals are same except slightly varied wavenumbers. This variation created by the addition of Rb in L-LMHCL.

3.3. EDX analysis

EDX is an analytical tool used to screen the chemical compositions of different elements in a solid sample and to determine the relative abundance of such chemical elements. The existence of Rb was confirmed without any doubt from EDX spectrum and is shown in Fig. 4. Moreover to these, carbon, oxygen and chlorides also exist in the grown crystal.

3.4. Optical analysis

The energy band structure, effect of impurity, excitons, localised defects and vibration of lattice can be studied with the aid of optical properties (Rajkumar and Praveen kumar 2019). The transmittance nature of the undoped and doped crystals are exposed in the Fig. 5a. Pure and doped crystals showed nearly 70 and 76 percentage of transmittance. Also doped crystal pronounced 6% higher transmission compared to pure. The dislocation in crystals mainly influences these optical properties. Because the lesser dislocation density contributes to the reduction of scattering centres of crystal, the transmission behaviour of Rb: L-LMHCL crystal was increased (Senthil Pandian et al., 2020). This led to the sample enroute for the fabrication of UV-tuneable laser device components. The energy dependency of the absorption coefficient (α) in the high energy region indicates the presence of a direct band gap that complies with the highest photon energy (hν) equation.

$$\alpha h\nu = A(h\nu - E_g)^{\frac{1}{2}} \quad (1)$$

The magnitude of the optical band gap (E_g) was 5.30 eV and 5.94 eV for pure and

Rb: L-LMHCL crystals respectively. It was found out from the intrigue between $(\alpha h\nu)^2$ versus hν and is represented in the Fig. 5b.

The loss of electromagnetic radiation, which is caused due to scattering and absorption in the crystal, is specified by its extinction coefficient value. Using following Equation. (2) extinction coefficient was calculated (Girisun and Dhanuskodi, 2009)

$$K = \frac{\lambda\alpha}{4\pi} \quad (2)$$

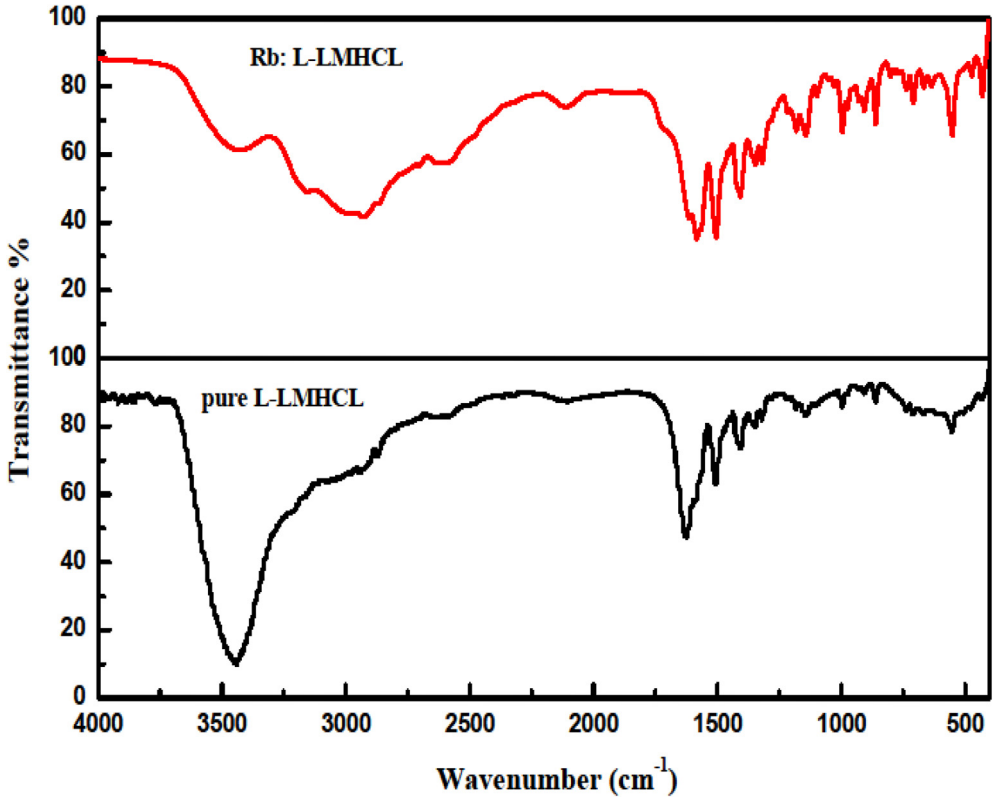

Fig. 3. FTIR spectra of Pure and Rb: L-LMHCL crystals.

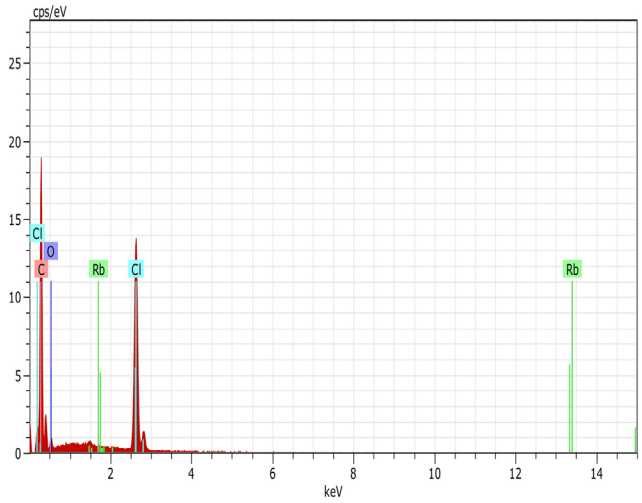

Fig. 4. EDX spectrum of Rb: L-LMHCL crystal.

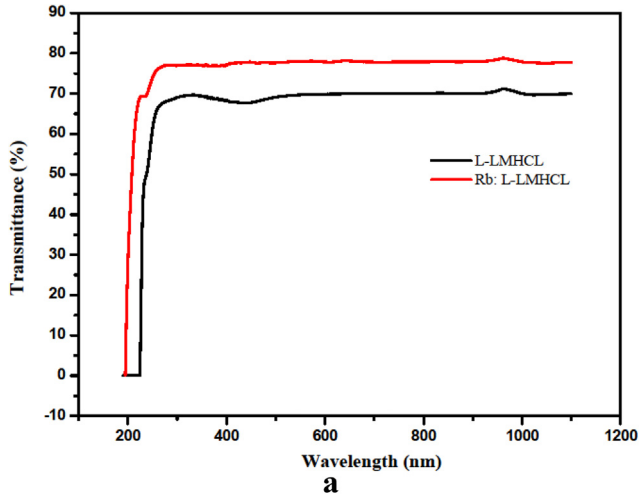

Fig. 5a. Percentage of transmittance of pure and Rb: L-LMHCL crystal.

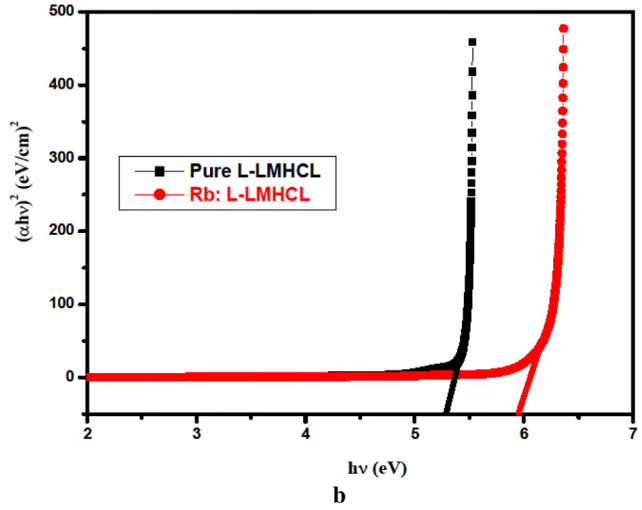

Fig. 5b. Band gap calculation of pure and Rb: L-LMHCL crystals using tauc plot.

In the Fig. 5c, the coefficient value attained to be lower for Rb: L-LMHCL. This indicates that there is less loss of radiation. However, when the photon energy is increased, the absorption and scattering takes place to some extent and this result in the increase of extinction coefficient. However, in the grown crystals the radiation passes without absorption in the visible region. For optical device applications, this is a desired property. Based on the amount of electromagnetic radiation penetrated into a material, skin depth (δ) was calculated by the Equation. (3) and the variation of skin depth with respect to photon energy is shown in Fig. 5d. The estimated value of the skin depth decreases with the increase of photon energy and the peak value shifted towards higher photo energy region comparing to pure. This result recommending the Rb: L-LMHCL crystal into wide range of optoelectronic applications.

$$\delta = \frac{1}{\alpha} \tag{3}$$

Another indispensable optical constant, the refractive index (n), plays a key role in the design of optical devices that enable knowledge of the local fields, polarisation and phase velocity of light in material propagation. The refractive index (n) can be estimated by the equation (4). in terms of transmittance (T) value.

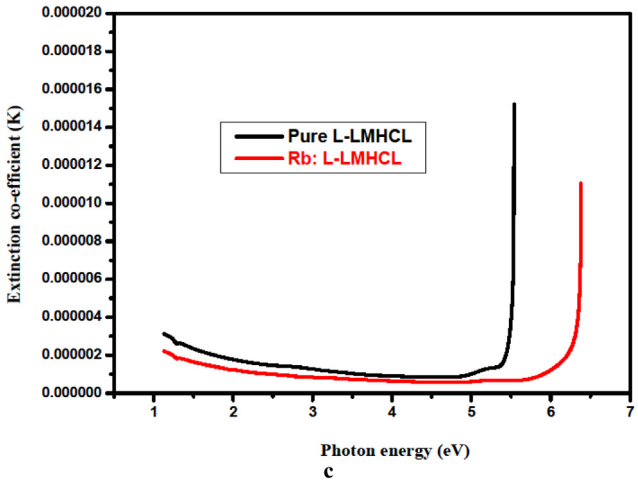

Fig. 5c. Extinction co-efficient of pure and Rb: L-LMHCL crystals.

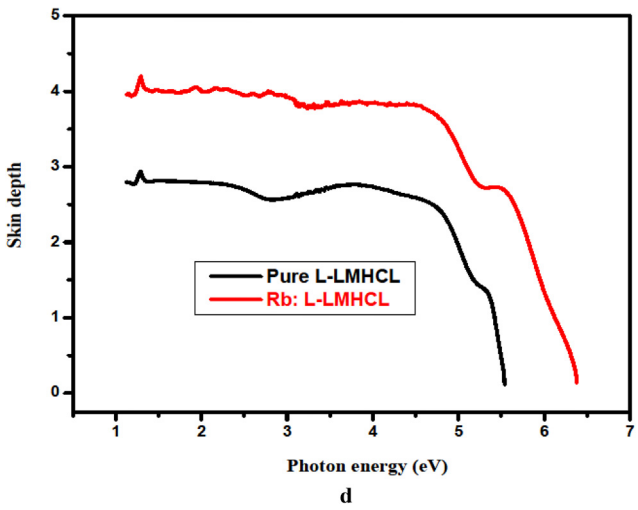

Fig. 5d. Skin depth of pure and Rb: L-LMHCL crystals.

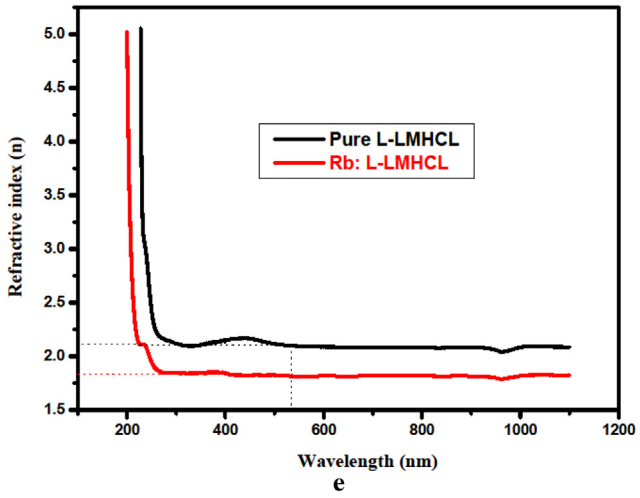

Fig. 5e. Refractive index of pure and Rb: L-LMHCL crystals.

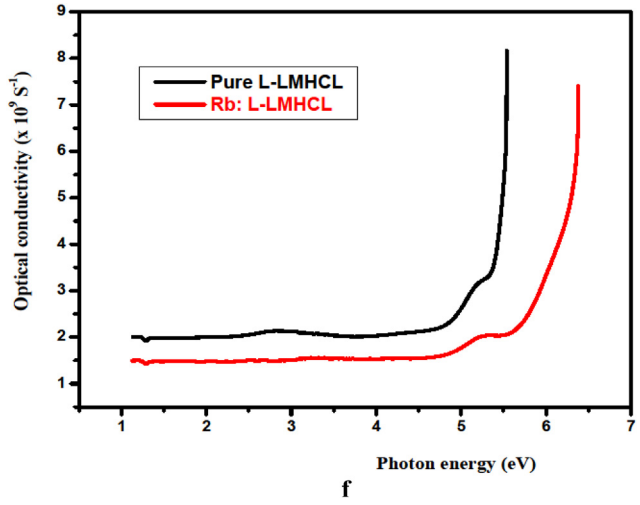

Fig. 5f. Optical conductivity of pure and Rb: L-LMHCL crystals.

$$n = \frac{1}{T} + \left(\frac{1}{T} - 1\right)^{\frac{1}{2}} \quad (4)$$

For the undoped and doped crystals, the magnitude of refractive index is decreased in accordance with the wavelength. The refractive index is found to be 1.82 for doped and 2.08 for pure at 532 nm (Fig. 5e). Rb: L-LMHCL is applicable in low dispersion and anti-reflection purpose of UV-light in solar thermal devices since the refractive index of doped is lower when compared to pure samples. The material's optical conductivity (σ_{op}) decided the use of the material in the optical field. The equation (5) gives optical conductivity. Fig. 5f elucidate that the optical conductivity increased due to the increase in photon energy. It confirms the better photo response of Rb: L-LMHCL crystal.

$$\sigma_{op} = \frac{\alpha n c}{4\pi} \quad (5)$$

3.5. Mechanical properties

The microhardness of the crystal acts a crucial role in the device application, which is characterized using Vickers microhardness measurement. Diverse factors such as debye temperature, interatomic lattice energy spacing, and heat of forming greatly influence the microhardness of crystal (Senthil et al., 2015). Many authors correlated the Surface energy, interatomic bonding, bond strength and lattice energy with the hardness of the crystals

(Kishan Rao and Sirdeshmukh 1983). Optically cracked free polished Rb added L-LMHCL crystal was used to carry out the hardness measurement. Diagonal length (d) was noted for different indentation loads such as 25, 50, 100 g. Using these datas, hardness (H_v) of crystal was calculated by the following Equation (6). and figure depicted the relation between load (P) and hardness.

$$H_v = \frac{1.8544p}{d^2}(Kg/mm^2) \quad (6)$$

Reverse Indentation Size Effect (RISE) is confirmed from the Fig. 6a. The hardness and mechanical strength of the doped L-LMHCL crystal is higher than that of the pure L-LMHCL crystal, which points out the incorporation of Rb in the lattice of pure L-LMHCL. Also this rise of mechanical strength elucidating the stability nature of the rare earth element rubidium chloride. The category of the material was found from the linear fit of log d and log p (Figs. 6b and 6c). This linear fit value, i.e., work hardening

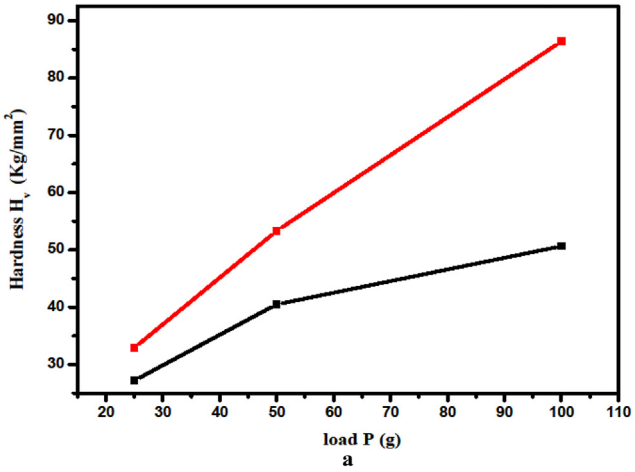

Fig. 6a. Hardness of pure and Rb: L-LMHCL crystals.

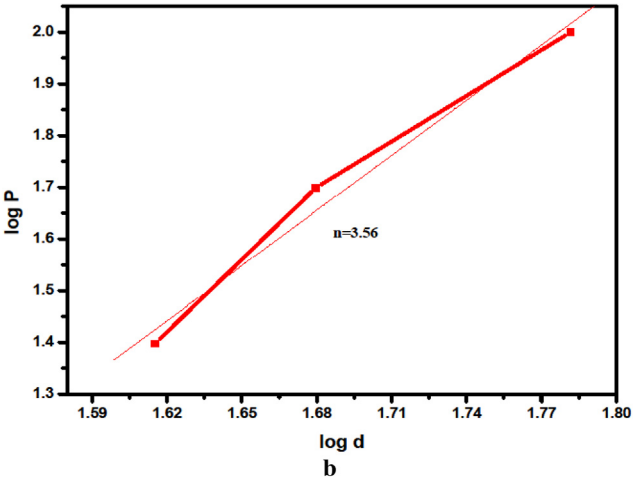

Fig. 6b. Plot of log d versus log P of pure crystal.

coefficient values such as 3.56 and 4.00 for L-LMHCL and Rb: L-LMHCL confirms that the materials are soft material regarding the view of Onitsch (Meyer, 1908).

In the field of structural engineering and device fabrication, the great concern is given to yield strength (σ_v) (Rajesh et al., 2019). Using Equation (7) yield strength can be found out (Kaliammal et al., 2020). Rb: L-LMHCL crystal shows good yield strength response (increases) to the increasing applied load and this response is shown in Fig. 6d.

$$\sigma_v = \frac{H_v}{2.9}\left\{[1-(n-2)]\left[\frac{12.5(n-2)}{(1-(n-2))}\right]^{n-2}\right\} \quad \text{for } n>2 \tag{7}$$

The bonding and strengthen behaviours with neighbouring atom can be known from the stiffness constant (C_{11}). It was emphasized by Wooster's empirical formula (Equation (8)) also this constant increases for raising loads and is shown in Fig. 6e (Wooster 1953). The bonding between adjacent atoms of Rb: L-LMHCL is superior as compared to the magnitude of pure L-LMHCL.

$$C_{11} = (H_v)^{7/4} \tag{8}$$

The capability of resisting fracture is known as fracture toughness (K_c) of the substance. Fracture toughness is one of the imperative parameters used for designing material. It was computed using the Equation (9) (Bamzai et al., 2000).

$$K_c = \frac{P}{\beta C^{3/2}} \tag{9}$$

In the above equation crack length is taken as 'C' and indentation geometry constant is denoted as 'β' its value is 7 for Vickers microhardness indentation. The response of fracture toughness to applied load is shown in Fig. 6f. The fracture caused without external force in the sample is described by Brittleness index (B_i). It was determined using Equation (10)

(Sangwal, 2009). The Brittleness index decreases gradually with increasing the load and this was known from the Fig. 6g.

$$B_i = \frac{H_v}{K_c} \tag{10}$$

Hardness, yield strength and stiffness constants are raised in Rb: L-LMHCL crystal than pure crystal. It shows the excessive strength power of Rb: L-LMHCL. The dopant Rb fills the Void of the L-LMHCL crystal owing to that only it has a high hardness number. Therefore, dislocation of crystal planes is strenuous because of the necessity of greater stress. This enhanced property reduces the wastage caused by breakage while polishing in the time of NLO device fabrication (Omegala priakumari et al., 2016).

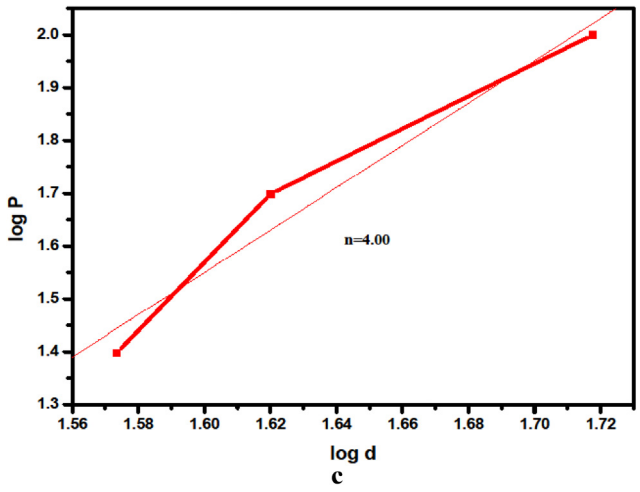

Fig. 6c. Plot of log d versus log P of Rb: L-LMHCL crystal.

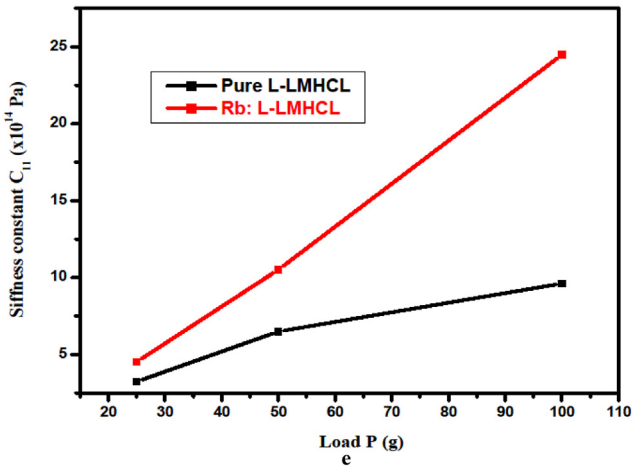

Fig. 6e. Stiffness constant of pure and Rb: L-LMHCL crystals.

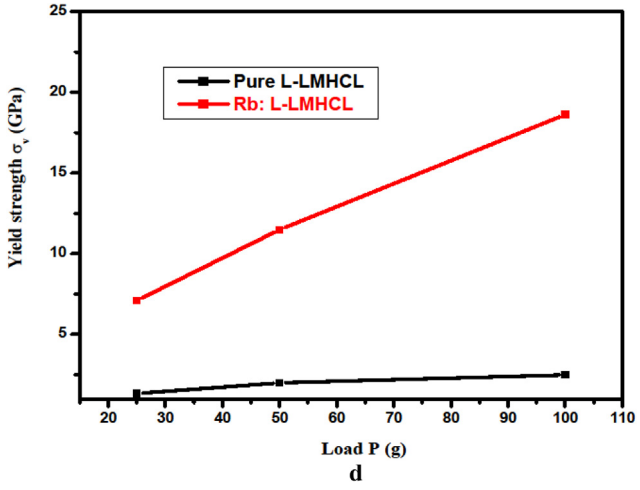

Fig. 6d. Yield strength of pure and Rb: L-LMHCL crystals.

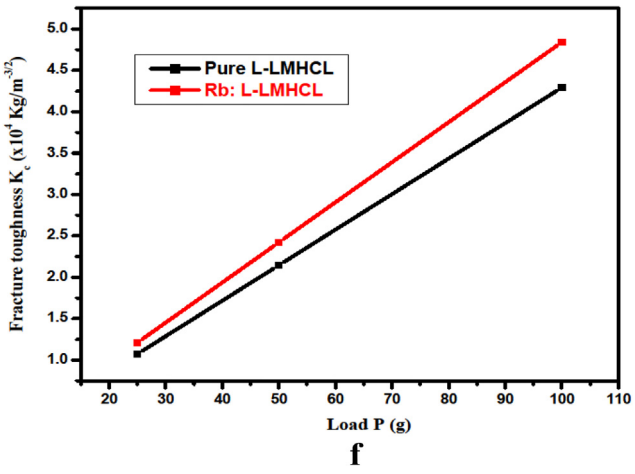

Fig. 6f. Fracture toughness of pure and Rb: L-LMHCL crystals.

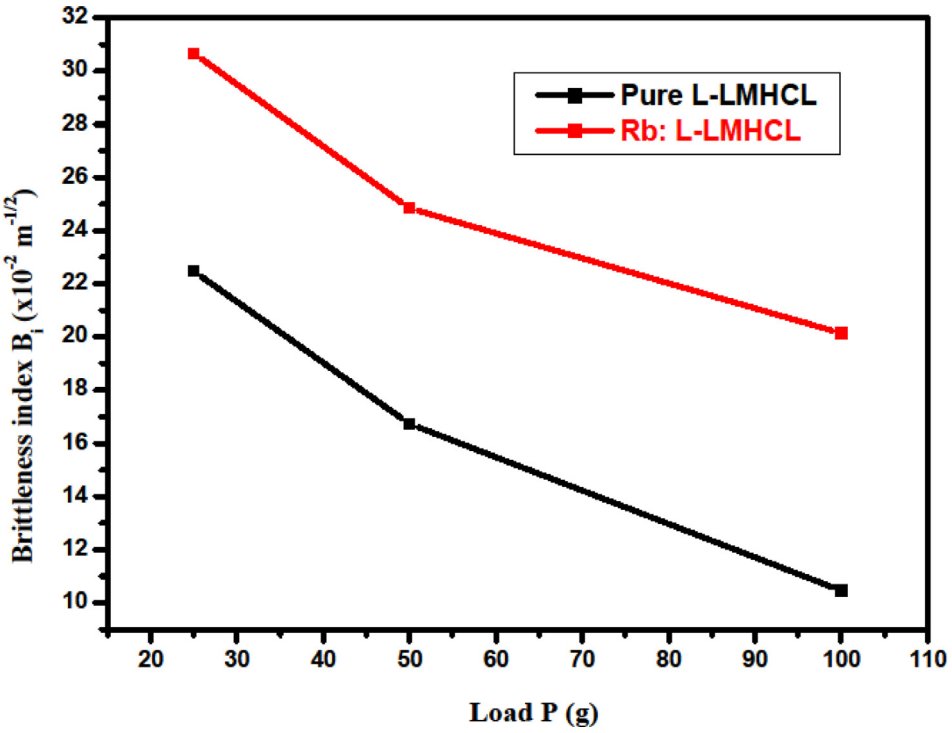

Fig. 6g. Brittleness index of pure and Rb: L-LMHCL crystals.

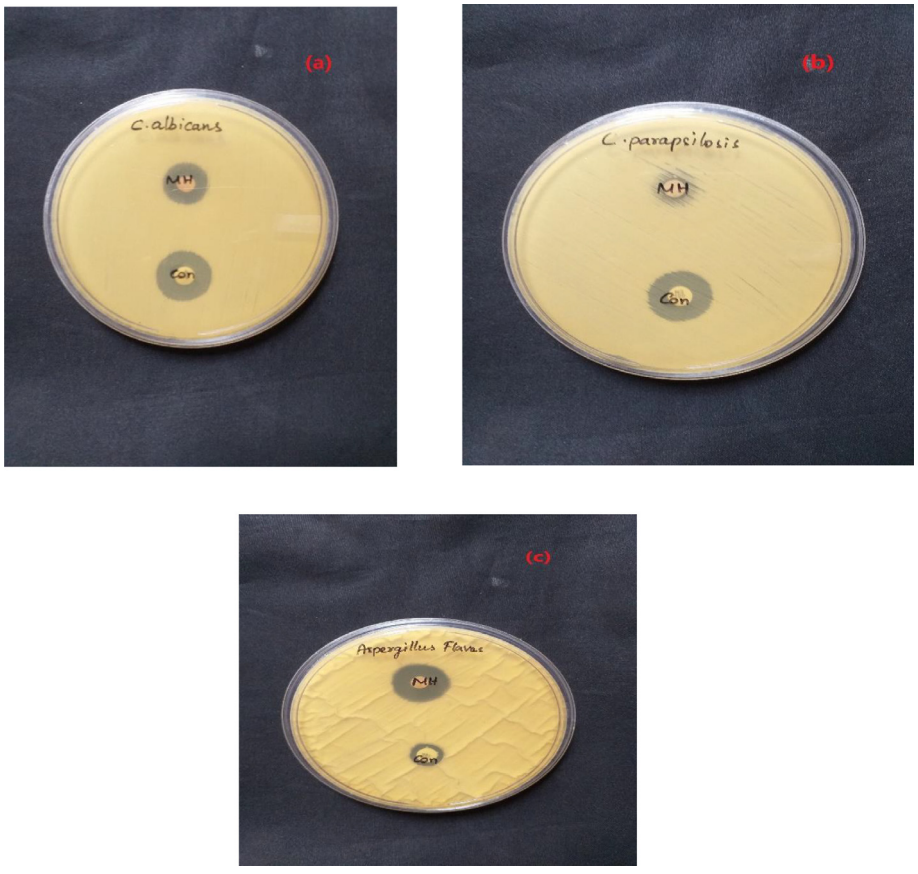

Fig. 7. Zone of inhibition of pure crystal against (a) *Candida albicans*, (b) *Candida parapsilosis* and (c) *Aspergillus flaves.*

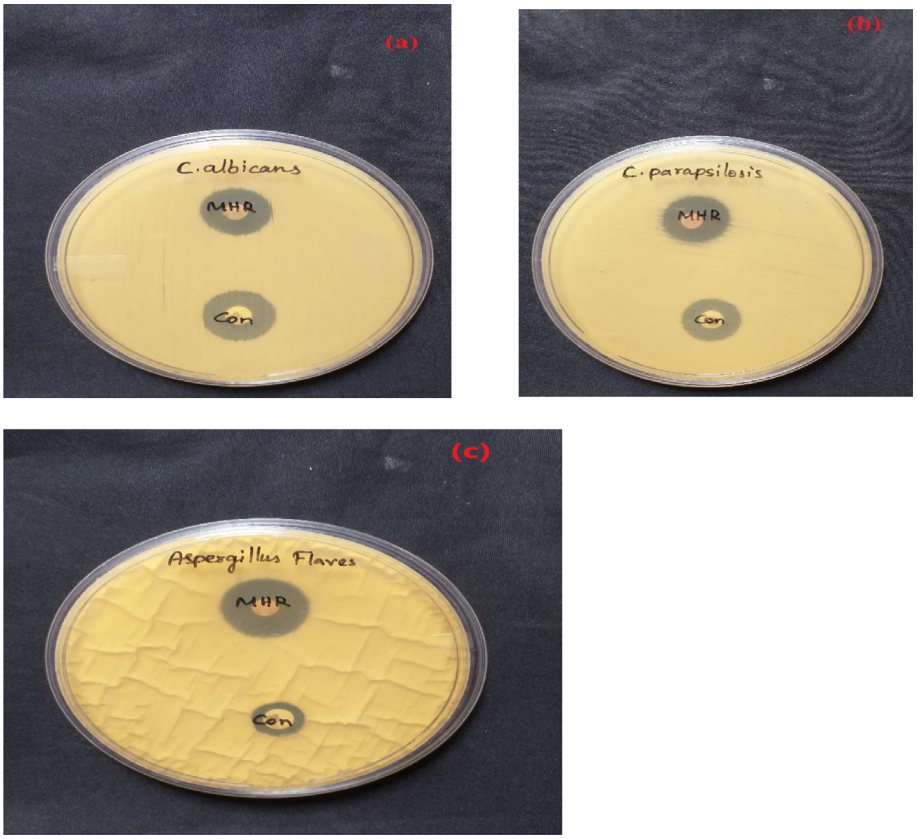

Fig. 8. Zone of inhibition of Rb: L-LMHCL crystal against (a) *Candida albicans*, (b) *Candida parapsilosis* and (c) *Aspergillus flaves*.

3.6. Nonlinear optical (NLO) property

To assess the NLO features of pure and Rb: L-LMHCL crystal, Kurtz and perry technique was carried out (Kurtz and Perry, 1968). Using high energy Nd: YAG laser, the materials were exposed and the resulting output signal was compared with the output signal of KDP. The outcome depicts that the pure and Rb: L-LMHCL crystals are 1.2 and 1.8 times greater than the efficiency of standard KDP. Ramya et al has been reported the L-Lysine adipate crystal with 0.62 times efficiency and Deepa et al reported nicotinic acid doped KDP crystal with 0.35 times SHG efficiency than KDP (Ramya et al., 2017, Deepa and Philominathan 2016).

3.7. Antifungal studies of pure and Rb doped L-LMHCL

In the last few decades, the major harmful health problem of human raised because of fungal infections. Among the fungal species, *Aspergillus*, *Candida* and *Cryptococcus* are the most frequent pathogens to motive about 1.5–2.0 million deaths every year (Ou et al., 2020). The major common source of urinary tract fungal infections (UTIs) is the Candida species (Behzadi et al., 2010). *Candida albicans* and *Aspergillus Flaves* species cause illness in immunocompromised persons (Iwen et al., 1997). *Aspergillus flavus* infected not only humans but also the agriculture crops. The growth of *Candida parapsilosis*, *Candida albicans*, and *Aspergillus Flaves* were prohibited by 15 mm, 10 mm, 20 mm diameter size by pure L-LMHCL crystal respectively (Fig. 7a). The prepared Rb: L-LMHCL material comparatively pronounced maximum susceptibility zone of 22 mm towards *Aspergilllus Flaves* among the three tested fungi and 19 mm least zone of inhibition was produced towards *Candida albicans*. Moreover, 20 mm range toxic produced against *Candida parapsilosis* (Fig. 8). In addition, antifungal activity of grown sample was high when comparing to standard antifungal drug nystatin. Thus, it is proved without any doubt that the grown compound can be used as a successful fungicide in the medical field.

4. Conclusion

The alkali halide (RbCl) doped L-LMHCL crystal was grown and characterized via different techniques like XRD, FTIR, and UV–Visible spectrometer. Similar monoclinic structure and $P2_1$ space group were obtained for both pure and Rb: L-LMHCL sample. At the same time, variation in intensity and shift in diffraction peaks were noticed from the powder XRD pattern. Also, scanty shift variation in the wavenumber of functional groups from pure crystal was assessed through FTIR. Optical behaviour of Rb: L-LMHCL crystal was enhanced because of Rb addition and band gap of pure and Rb: L-LMHCL are 5.52 eV and 6.37 eV. Presence of Rubidium in the L-LMHCL was also authenticated by EDX spectrum. Mechanical properties like hardness, yield strength and stiffness constants were increased than pure crystal by the addition of RbCl. Work hardening coefficient revealed the soft nature of materials. Grown crystal pronounced the antifungal activities against pathogens than the standard antifungal drug. Overall result exposes the enhanced optical, mechanical and antifungal performance of Rb: L-LMHCL crystal as well as the application in the field of photonics and medicine.

Funding

The authors are grateful to the technical support from Laboratory STIC, Cochin, SAIF, IIT, Chennai, and St. Joseph College, Tiruchirappalli. The authors thank Nesamony Memorial Christian College

for providing the facility to perform the experiment. The authors extend their appreciation to Taif University for funding current work by Taif University Researchers Supporting Project number (TURSP-2020/295), Taif University, Taif, Saudi Arabia.

Declaration of Competing Interest

The authors declare that they have no known competing financial interests or personal relationships that could have appeared to influence the work reported in this paper.

Acknowledgements

The authors are grateful to the technical support from Laboratory STIC, Cochin, SAIF, IIT, Chennai, and St. Joseph College, Tiruchirappalli. The authors thank Nesamony Memorial Christian College for providing the facility to perform the experiment. The authors extend their appreciation to Taif University for funding current work by Taif University Researchers Supporting Project number (TURSP-2020/295), Taif University, Taif, Saudi Arabia.

References

Anis, M., Muley, G.G., Baig, M.I., Rabbani, G., Ghramh, H.A., Ramteke, S.P., 2018. Doping effect of Ni2+ on structural, UV-visible, SHG efficiency, dielectric and microhardness traits of KH2PO4 (KDP) crystal. Optik. 178, 752–757.

Bamzai, K.K., Kotru, P.N., Wanklyn, B.M., 2000. Fracture mechanics, crack propagation and microhardness studies on flux grown ErAlO3 single crystals. J. Mater. Sci. Technol. 16 (4), 405–410.

Behzadi, P., Behzadi, E., Yazdanbod, H., Aghapour, R., Cheshmeh, M.A., Omran, D., 2010. Urinary tract infections associated with Candida albicans. Maedica – A. J Clin. Med. 5 (4), 277–279.

Boopathi, K., Jagan, R., Ramasamy, P., 2016. Synthesis, crystal growth and characterizations of bis (l-proline) cadmium iodide: a new semi-organic nonlinear optical material. Appl. Phys. A 122 (7), 183–186.

Deepa, B., Philominathan, P., 2016. Enhanced NLO and antibacterial properties of nicotinic acid-doped KDP crystals: synthesis, growth and characterisation. Mater. Res. Innov. 21 (2), 86–90.

Elamathi, R., Ramesh, R., Aravinthraj, M., Manivannan, M., Liakath Ali Khan, F., Mphale, K., Maaza, M. (2020). Investigation of structural and electrical properties of lithium cobalt oxide nanoparticles for optoelectronic applications. Surfaces and Interfaces, 20, 100582.

Ertan, B., 2017. Extraction of rubidium from natural resources. AIP Conf. Proc. 1833, (1) 020084.

Fan, Y., Li, D., Gao, D., Zeng, D., Li, W., 2020. Heat capacity of Rb2SO4 (aq) and Cs2SO4 (aq) solutions and thermodynamic modelling of (Rb2SO4 + H2O) and (Cs2SO4 + H2O) systems. J. Chem. Thermodyn. 142, 106001.

Fieve, R.R., Meltzer, H.L., Taylor, R.M., 1971. Rubidium chloride ingestion by volunteer subjects: Initial experience. Psychopharmacology 20 (4), 307–314.

Girisun, T.C.S., Dhanuskodi, S., 2009. Linear and nonlinear optical properties of tris thiourea zinc sulphate single crystals. Cryst. Res. Technol. 44 (12), 1297–1302.

Iwen, PC., Rupp., Hinrichs., ME, SH., 1997. Invasive Mold Sinusitis: 17 Cases in Immunocompromised Patients and Review of the Literature. Clin. Infect. Dis. 24 (6), 1178–1184.

Kaliammal, R., Sudhahar, S., Parvathy, G., Velsankar, K., Sankaranarayanan, K., 2020. Physicochemical and DFT studies on new organic Bis-(2-amino-6-methylpyridinium) succinate monohydrate good quality single crystal for nonlinear optical applications. J. Mol. Struct. 1212, 128069.

Kandasamy, A., Mohan, R., Lydia Caroline, M., Vasudevan, S., 2008. Nucleation kinetics, growth, solubility and dielectric studies of L-proline cadmium chloride monohydrate semi organic nonlinear optical single crystal. Cryst. Res. Technol. 43 (2), 186–192.

Kandhan, S., Arasan, B.T., Jagan, R., Aravindhan, S., Srinivasan, S., Anbalagan, S., 2020. Structural, linear and non linear optical, electrical, piezoelectric and thermal investigation on new semi-organic single crystal for microelectronics and high power laser applications: A brucinium di-hydrogen borate hydrate. Opt. Mater. 109, 110261.

Kimura, H., Tanahashi, R., Zhao, H., Maiwa, K., 2010. Crystal growth and electric-property change by rubidium or cesium doping on potassium-sodium-niobate. Cryst. Res. Technol. 46 (1), 37–40.

Kishan Rao, K., Sirdeshmukh, D.B., 1983. Microhardness and interatomic binding in some cubic crystals. Bull. Mater. Sci. 5 (5), 449–452.

Kurtz, S.K., Perry, T.T., 1968. A powder technique for the evalution of nonlinear optical materials. Int. J. Appl. Phys. 39, 3798–3813.

Lucia Rose, A.S.J., Selvarajan, P., Perumal, S., 2011. Growth, structural, spectral, mechanical and dielectric characterization of RbCl-doped l-alanine hydrogen chloride monohydrate single crystal. Physica B Condens. Matter. 406 (3), 412–417.

Malek-Ahmadi, P., Williams, J.A., 1984. Rubidium in psychiatry: Research implications. Pharmacol. Biochem. Behav. 21, 49–50.

Meyer, E., 1908. Contribution to the knowledge of hardness and hardness testing. Z. Ver. Dtsch. Ing. 52 (1908), 740–835.

Omegala priakumari., R, Grace Sahaya Sheba, S., Gunasekaran, M., 2016. Growth and characterisation of l-lysine hydrochlorobromide (LYHCBr), a novel semiorganic non-linear optical (NLO) single crystal. Mater. Res. Innov. 20, 177-181.

Ou, Y.H., Du, R.K., Zhang, S.P., Ling, Y., Li, S., Zhao, C.J., Zhang, L., 2020. Synthesis, crystal structure and in vitro antifungal activity of two-dimensional silver(I)-voriconazole coordination complexes. J. Mol. Struct. 1215, 128229.

Ouyang, S., Zheng, K., Huang, Q., Liu, Y., Boccaccini, A.R., 2020. Synthesis and characterization of rubidium-containing bioactive glass nanoparticles. Mater. Lett. 273, 127920.

Park, I.J., Seo, S., Park, M.A., Lee, S., Kim, D.H., Zhu, K., Kim, J.Y., 2017. Effect of Rubidium Incorporation on the Structural, Electrical, and Photovoltaic Properties of Methylammonium Lead Iodide-Based Perovskite Solar Cells. ACS Appl. Mater. Interfaces 9 (48), 41898–41905.

Paschalis, C., Jenner, F.A., Lee, C.R., 1978. Effects of Rubidium Chloride on the Course of Manic-Depressive Illnesses. J. R. Soc. Med. 71 (5), 343–352.

Rajesh, K., Krishnan, P., Mani, A., Anandan, K., Gayathri, K., Devendran, P., 2019. Physical strength and Opto-electrical conductivity of L-Serine Phosphate single crystal for structural and photonics devices fabrication. Mater. Res. Innov. 24, 295–300.

Rajkumar, R., Praveen Kumar, P., 2019. Structure, crystal growth and characterization of piperazinium bis(4-nitrobenzoate) dihydrate crystal for nonlinear optics and optical limiting applications. J. Mol. Struct. 1179, 108–117.

Ramya, K., Saraswathi, N.T., Raja, C.R., 2017. Growth and characterization of L-Lysine adipate crystal. Opt. Laser Technol. 90, 222–225.

Ravi, S., Sreedharan, R., Raghi, K.R., Manoj Kumar, T.K., Naseema, K., 2021. Studies on non-linear optical property of β polymorph of 5-nitrofurazone- a promising optical material: Experimental and Quantum Computational approach. Chem. Phys. Lett. 763, 138161.

Sangwal, K., 2009. Review: Indentation size effect, indentation cracks and microhardness measurement of brittle crystalline solids - some basic concepts and trends. Cryst. Res. Technol. 44 (10), 1019–1037.

Senthil Pandian, M., Verma, S., Ramasamy, P., Singh, G., Gupta, S.M., Tiwari, V.S., Karnal, A.K., 2020. Growth of [010] oriented urea-doped triglycine sulphate (Ur-TGS) single crystals below and above Curie temperature (Tc) and comparative investigations of their physical properties. Appl. Phys. A 126 (7), 492.

Senthil, K., Kalainathan, S., Hamada, F., Kondo, Y., 2015. Bulk crystal growth and nonlinear optical characterization of a stilbazolium derivative crystal: 4-[2-(3, 4 dimethoxyphenyl) ethenyl]-l methylpyridinium tetraphenylborate (DSTPB) for NLO device fabrication. RSC Adv. 5 (97), 79298–79308.

Wooster, W.A., 1953. Properties and atomic arrangements in crystals. Rep. Prog. Phys. 16, 62–82.

Yusof, S.M., Pang, Z.B., Teh, L.P., 2020. Fibrous silica HZSM-5 towards CO2 adsorption performance: Effect of copper oxide loading. Mater. Today 31 (1), 155–160.